

Disk Winds, Jets, and Outflows: Theoretical and Computational Foundations

Ralph E. Pudritz

McMaster University

Rachid Ouyed

University of Calgary

Christian Fendt

Max-Planck Institute for Astronomy, Heidelberg

Axel Brandenburg

Nordic Institute for Theoretical Physics

We review advances in the theoretical and computational studies of disk winds, jets and outflows including: the connection between accretion and jets, the launch of jets from magnetized disks, the coupled evolution of jets and disks, the interaction of magnetized young stellar objects with their surrounding disks and the relevance to outflows, and finally, the link between jet formation and gravitational collapse. We also address the predictions that the theory makes about jet kinematics, collimation, and rotation, that have recently been confirmed by high spatial and spectral resolution observations. Disk winds have a universal character that may account for jets and outflows during the formation of massive stars as well as brown dwarfs.

1. INTRODUCTION

The close association of jets and outflows with protostellar accretion disks is one of the hallmarks of the accretion picture of low mass star formation. The most energetic outflow phase occurs during gravitational collapse of a molecular cloud core - the so-called Class 0 phase - when much of its envelope is still raining down onto the forming protostellar disk and the disk accretion rate is high. Later, in the T-Tauri star (TTS) stage, when most of the original core has been accreted and the young stellar object (YSO) is being fed by lower accretion rates through the surrounding Keplerian accretion disk, the high-speed jet becomes optically visible. When the disk disappears in the weak-lined TTS (WTTS) phase, the jet goes with it.

The most comprehensive theoretical picture that we have for these phenomena is that jets are highly collimated, hydromagnetic disk winds whose torques efficiently extract disk angular momentum and gravitational potential energy. Jets also sweep up ambient molecular gas and drive large scale molecular outflows. A disk wind was first suggested as the origin of jets from accretion disks around black holes in the seminal paper by *Blandford and Payne* (1982, BP82), and was soon proposed as the mechanism for protostellar jets (*Pudritz and Norman*, 1983, 1986).

Several major observational breakthroughs have taken place in the study of jets and outflows since PPIV (held in 1998). Direct, high resolution spectro-imaging and adaptive optics methods discovered the rotation of protostellar

jets (*Bacciotti et al.*, 2003). These observations also revealed that jets have an onion-like, velocity structure (with the highest speeds being closest to the outflow axis). This work provides strong support for the idea that jets originate as centrifugally driven MHD winds from extended regions of their surrounding disks (see chapter by *Ray et al.*). Recently, outflows and disks have also been discovered around massive stars (see chapter by *Arce et al.*) as well as brown dwarfs (e.g., *Bourke et al.* 2005) implying that the mechanism is important across the entire stellar mass spectrum.

Major advances in the theoretical modeling of these systems have also occurred, due primarily to a variety of MHD computational studies. Simulations now resolve the global evolution of disks and outflows, track the interaction of disks with central magnetized stars, and even follow the generation of outflows during gravitational collapse. These studies show that jets and disks are closely coupled and that jet dynamics scales to YSOs of all masses.

Our review examines the theory of the central engine of jets and its exploration through the use of computer simulations. We focus mainly on developments since PPIV and refer to the review by *Königl and Pudritz* (2000, KP00) for a discussion of the earlier literature, as well as *Pudritz* (2003) and *Heyvaerts* (2003) for more technical background. We first discuss the basic theory of disk winds and their kinematics. We then switch to computational studies of jets from accretion disks treated as boundary conditions, as well as global simulations including the disk. We then examine

the innermost regions of the disk where the stellar magnetosphere interacts with the disk, as well as the surface of the star that may drive an accretion-powered outflow. Finally, we discuss how outflows are generated during the early stages of the gravitational collapse.

2. THEORY OF DISK WINDS

An important insight into the nature of the engine for jets can be gleaned from the observed ratio of the momentum transport rate (or thrust) carried by the CO molecular outflow to the thrust that can be provided by the bolometric luminosity of the central star (e.g., *Cabrit and Bertout, 1992*);

$$F_{\text{outflow}}/F_{\text{rad}} = 250(L_{\text{bol}}/10^3L_{\odot})^{-0.3}, \quad (1)$$

This relation has been confirmed and extended by the analysis of data from over 390 outflows, ranging over six decades up to 10^6L_{\odot} in stellar luminosity (*Wu et al., 2004*). It suggests that jets from both low and high mass systems are probably driven by a single, non-radiative, mechanism.

Jets are observed to have a variety of structures and time-dependent behaviour – from internal shocks and moving knots to systems of bow shocks that suggest long-time episodic outbursts. They show wiggles and often have cork-screw like structure, suggesting the presence either of jet precession, the operation of non-axisymmetric kink modes, or both. Given the highly nonlinear behaviour of the force balance equation for jets (the so-called Grad-Shafranov equation), theoretical work has focused on tractable and idealized time-independent, and axisymmetric or self-similar models (e.g., BP82) of various kinds.

2.1. Conservation Laws and Jet Kinematics

Conservation laws are the gold standard in physics, and play a significant role in understanding astrophysical jets. This is because whatever the details (e.g. the asymptotics, the crossing of critical points, the way that matter is loaded onto field lines within the disks, etc.), conservation laws strongly constrain the flux of mass, angular momentum, and energy. What cannot be constrained by these laws will depend on the general physics of the disks such as on how matter is loaded onto field lines.

Jet dynamics can be described by the time-dependent, equations of ideal MHD. The evolution of a magnetized, rotating system that is threaded by a large-scale field \mathbf{B} involves (i) the continuity equation for a conducting gas of density ρ moving at velocity \mathbf{v} (which includes turbulence); (ii) the equation of motion for the gas which undergoes pressure (p), gravitational (with potential Φ), and Lorentz forces; (iii) the induction equation for the evolution of the magnetic field in the moving gas where the current density is $\mathbf{j} = (c/4\pi)\nabla \times \mathbf{B}$; (iv) the energy equation, where e is the internal energy per unit mass; and, (v) the absence of magnetic monopoles. These are written as:

$$\frac{\partial \rho}{\partial t} + \nabla \cdot (\rho \mathbf{v}) = 0 \quad (2)$$

$$\rho \left(\frac{\partial \mathbf{v}}{\partial t} + (\mathbf{v} \cdot \nabla) \mathbf{v} \right) + \nabla p + \rho \nabla \Phi - \frac{\mathbf{j} \times \mathbf{B}}{c} = 0 \quad (3)$$

$$\frac{\partial \mathbf{B}}{\partial t} - \nabla \times (\mathbf{v} \times \mathbf{B}) = 0 \quad (4)$$

$$\rho \left(\frac{\partial e}{\partial t} + (\mathbf{v} \cdot \nabla) e \right) + p(\nabla \cdot \mathbf{v}) = 0 \quad (5)$$

$$\nabla \cdot \mathbf{B} = 0 \quad (6)$$

We specialize to the restricted case of stationary, as well as 2D (axisymmetric) flows, from which the conservation laws follow. It is useful to decompose vector quantities into poloidal and toroidal components (e.g. magnetic field $\mathbf{B} = \mathbf{B}_p + B_{\phi} \hat{\mathbf{e}}_{\phi}$). In axisymmetric conditions, the poloidal field \mathbf{B}_p can be derived from a single scalar potential $a(r, z)$ whose individual values, $a = \text{const}$, define the surfaces of constant magnetic flux in the outflow and can be specified at the surface of the disk (e.g., *Pelletier and Pudritz, 1992; PP92*).

Conservation of mass and magnetic flux along a field line can be combined into a single function k that is called the “mass load” of the wind which is a constant along a magnetic field line;

$$\rho \mathbf{v}_p = k \mathbf{B}_p. \quad (7)$$

This function represents the mass load per unit time, per unit magnetic flux of the wind. For axisymmetric flows, its value is preserved on each ring of field lines emanating from the accretion disk. Its value on each field line is determined by physical conditions - including dissipative processes - near the disk surface. It may be more revealingly written as

$$k(a) = \frac{\rho v_p}{B_p} = \frac{d\dot{M}_w}{d\Psi}, \quad (8)$$

where $d\dot{M}_w$ is the mass flow rate through an annulus of cross-sectional area dA through the wind and $d\Psi$ is the amount of poloidal magnetic flux threading through this same annulus. The mass load profile is a function of the footpoint radius r_0 of the wind on the disk.

The toroidal field in rotating flows derives from the induction equation;

$$B_{\phi} = \frac{\rho}{k} (v_{\phi} - \Omega_0 r), \quad (9)$$

where Ω_0 is the angular velocity of the disk at the mid-plane. This result shows that the strength of the toroidal field in the jet depends on the mass loading as well as the jet density. Denser winds should have stronger toroidal fields. We note however, that the density does itself depend on the value of k . Equation (9) also suggests that at higher mass loads, one has lower toroidal field strengths. This can be reconciled however, since it can be shown from the conservation laws (see below) that the value of k is related to the density of the outflow at the Alfvén point on a field line; $k = (\rho_A/4\pi)^{1/2}$ (e.g., PP92). Thus, higher mass loads correspond to denser winds and when this is substituted into

equation (9), we see that this also implies stronger toroidal fields. We show later that jet collimation depends on hoop stress through the toroidal field and thus the mass load must have a very important effect on jet collimation (Section 3.2).

Conservation of angular momentum along each field line leads to the conserved angular momentum per unit mass;

$$l(a) = rv_\phi - \frac{rB_\phi}{4\pi k} = \text{const.} \quad (10)$$

The form for l reveals that the total angular momentum is carried by both the rotating gas (first term) as well by the twisted field (second term), the relative proportion being determined by the mass load.

The value of $l(a)$ that is transported along each field line is fixed by the position of the Alfvén point in the flow, where the poloidal flow speed reaches the Alfvén speed for the first time ($m_A = 1$). It is easy to show that the value of the specific angular momentum is;

$$l(a) = \Omega_0 r_A^2 = (r_A/r_0)^2 l_0. \quad (11)$$

where $l_0 = v_{K,0} r_0 = \Omega_0 r_0^2$ is the specific angular momentum of a Keplerian disk. For a field line starting at a point r_0 on the rotor (disk in our case), the Alfvén radius is $r_A(r_0)$ and constitutes a lever arm for the flow. The result shows that the angular momentum per unit mass that is being extracted from the disk by the outflow is a factor of $(r_A/r_0)^2$ greater than it is for gas in the disk. For typical lever arms, one particle in the outflow can carry the angular momentum of ten of its fellows left behind in the disk.

Conservation of energy along a field line is expressed as a generalized version of Bernoulli's theorem (this may be derived by taking the dot product of the equation of motion with \mathbf{B}_p). Thus, there is a specific energy $e(a)$ that is a constant along field lines, which may be found in many papers (e.g., BP82 and PP92). Since the terminal speed $v_p = v_\infty$ of the disk wind is much greater than its rotational speed, and for cold flows, the pressure may also be ignored, one finds the result:

$$v_\infty \simeq 2^{1/2} \Omega_0 r_A = (r_A/r_0) v_{\text{esc},0}. \quad (12)$$

There are three important consequences for jet kinematics here; (i) that the terminal speed exceeds the local escape speed from its launch point on the disk by the lever arm ratio; (ii) the terminal speed scales with the Kepler speed as a function of radius, so that the flow will have an onion-like layering of velocities, the largest inside, and the smallest on the larger scales, as seen in the observations; and (iii) that the terminal speed depends on the depth of the local gravitational well at the footpoint of the flow – implying that it is essentially scalable to flows from disks around YSOs of any mass and therefore universal.

Another useful form of the conservation laws is the combination of energy and angular momentum conservation to produce a new constant along a field line (e.g., PP92); $j(a) \equiv e(a) - \Omega_0 l(a)$. This expression has been used (Anderson *et al.*, 2003) to deduce the rotation rate of the launch

region on the Kepler disk, where the observed jet rotation speed is $v_{\phi,\infty}$ at a radius r_∞ and which is moving in the poloidal direction with a jet speed of $v_{p,\infty}$. Evaluating j for a cold jet at infinity and noting that its value (calculated at the foot point) is $j(a_0) = -(3/2)v_{K,0}^2$, one solves for the Kepler rotation at the point on the disk where this flow was launched:

$$\Omega_0 \simeq v_{p,\infty}^2 / (2v_{\phi,\infty} r_\infty). \quad (13)$$

When applied to the observed rotation of the Large Velocity Component (LVC) of the jet DG Tau (Bacciotti *et al.*, 2002), this yields a range of disk radii for the observed rotating material in the range of disk radii, 0.3–4 AU, and the magnetic lever arm is $r_A/r_0 \simeq 1.8\text{--}2.6$.

2.2. Angular Momentum Extraction

How much angular momentum can such a wind extract from the disk? The angular momentum equation for the accretion disk undergoing an external magnetic torque may be written:

$$\dot{M}_a \frac{d(r_0 v_0)}{dr_0} = -r_0^2 B_\phi B_z|_{r_0,H}, \quad (14)$$

where we have ignored transport by MRI turbulence or spiral waves. By using the relation between poloidal field and outflow on the one hand, as well as the link between the toroidal field and rotation of the disk on the other, the angular momentum equation for the disk yields one of the most profound scaling relations in disk wind theory – namely – the link between disk accretion and mass outflow rate (see KP00, PP92 for details):

$$\dot{M}_a \simeq (r_A/r_0)^2 \dot{M}_w. \quad (15)$$

The observationally well known result that in many systems, $\dot{M}_w/\dot{M}_a \simeq 0.1$ is a consequence of the fact that lever arms are often found in numerical and theoretical work to be $r_A/r_0 \simeq 3$ – the observations of DG Tau being a perfect example. Finally, we note that the angular momentum that is observed to be carried by these rotating flows (e.g. DG Tau) is a consistent fraction of the excess disk angular momentum – from 60–100% (e.g., Bacciotti, 2004), which is consistent with the high extraction efficiency discussed here.

2.3. Jet Power and Universality

These results can be directly connected to the observations of momentum and energy transport in the molecular outflows. Consider the total mechanical power that is carried by the jet, which may be written as (e.g., Pudritz, 2003);

$$L_{\text{jet}} = \frac{1}{2} \int_{r_i}^{r_j} d\dot{M}_w v_\infty^2 \simeq \frac{GM_* \dot{M}_a}{2r_i} \left(1 - \frac{r_i^2}{r_j^2} \right) \simeq \frac{1}{2} L_{\text{acc}}. \quad (16)$$

This explains the observations of Class 0 outflows wherein $L_w/L_{\text{bol}} \simeq 1/2$, since the main luminosity of the central

source at this time is due to accretion and not nuclear reactions. (The factor of 1/2 arises from the dissipation of some accretion energy as heat at the inner boundary). The ratio of wind to stellar luminosity decreases at later stages because the accretion luminosity becomes relatively small compared to the bolometric luminosity of the star as it nears the ZAMS.

This result states that the wind luminosity taps the gravitational energy release through accretion in the gravitational potential of the central object – and is a direct consequence of Bernoulli’s theorem. This, and the previous results, imply that jets may be produced in any accreting system. The lowest mass outflow that has yet been observed corresponds to a proto-brown dwarf of luminosity $\simeq 0.09L_\odot$, a stellar mass of only $20 - 45M_{Jup}$, and a very low mass disk $< 10^{-4}M_\odot$ (Bourke *et al.*, 2005).

It should be possible, therefore, for lower luminosity jets to be launched from the disks around Jovian mass planets. Recent hydrodynamical simulations of circumstellar accretion disks containing and building up an orbiting protoplanetary core have numerically proven the existence of a circum-planetary sub-disk in almost Keplerian rotation close to the planet (Kley *et al.*, 2001). The accretion rate of these sub-disks is about $\dot{M}_{cp} = 6 \times 10^{-5} M_{Jup} \text{ yr}^{-1}$ and is confirmed by many independent simulations. With that, the circum-planetary disk temperature may reach values up to 2000 K indicating a sufficient degree of ionization for matter-field coupling and would also allow for strong equipartition field strength (Fendt, 2003).

The possibility of a planetary scale MHD outflow, similar to the larger scale YSO disk winds, is indeed quite likely because: (i) the numerically established existence of circum-planetary disks is a natural feature of the formation of massive planets; and (ii) the feasibility of a large-scale magnetic field in the protoplanetary environment (Quillen and Trilling, 1998; Fendt, 2003). One may show, moreover, that the outflow velocity is of the order of the escape speed for the protoplanet, at about 60 km s^{-1} (Fendt, 2003).

On very general grounds, disk winds are also likely to be active during massive star formation (e.g., Königl 1999). Such outflows may already start during the early collapse phase when the central YSO still has only a fraction of a solar mass (e.g., Pudritz and Banerjee, 2005). Such early outflows may actually enhance the formation of massive stars via disk accretion by punching a hole in the infalling envelop and releasing the building radiation pressure (e.g., Krumholz *et al.*, 2005).

2.4. Jet Collimation

In the standard picture of hydromagnetic winds, collimation of an outflow occurs because of the increasing toroidal magnetic field in the flow resulting from the inertia of the gas. Beyond the Alfvén surface, equation (8) shows that the ratio of the toroidal field to the poloidal field in the jet is of the order $B_\phi/B_p \simeq r/r_A \gg 1$, so that the field becomes highly toroidal. In this situation, collimation is

achieved by the tension force associated with the toroidal field which leads to a radially inwards directed component of the Lorentz force (or “z-pinch”); $F_{\text{Lorentz},r} \simeq j_z B_\phi$. The stability of such systems is examined in the next section.

In Heyvaerts and Norman (1989) it was shown that two types of solution are possible depending upon the asymptotic behaviour of the total current intensity in the jet;

$$I = 2\pi \int_0^r j_z(r', z') dr' = (c/2)rB_\phi. \quad (17)$$

In the limit that $I \rightarrow 0$ as $r \rightarrow \infty$, the field lines are paraboloids which fill space. On the other hand, if the current is finite in this limit, then the flow is collimated to cylinders. The collimation of a jet therefore depends upon its current distribution – and hence on the radial distribution of its toroidal field – which, as we saw earlier, depends on the mass load. Mass loading therefore must play a very important role in controlling jet collimation.

It can be shown (Pudritz *et al.*, 2006; PRO) that for a power law distribution of the magnetic field in the disk, $B_z(r_0, 0) \propto r_0^{\mu-1}$ and an injection speed at the base of a (polytropic) corona that scales as the Kepler speed, that the mass load takes the form $k \propto r_o^{-1-\mu}$. In this regime, the current takes the form $I(r, z) \propto r_o^{-\mu-(1/2)}$. Thus, the current goes to zero for models with $\mu < -1/2$, and that these therefore must be wide angle flows. For models with $\mu > -1/2$ however, the current diverges, and the flow should collimate to cylinders.

These results predict that jets should show different degrees of collimation depending on how they are mass loaded (PRO). As an example, neither the highly centrally concentrated, magnetic field lines associated with the initial split-monopole magnetic configuration used in simulations by Romanova *et al.* (1997), nor the similar field structure invoked in the X-wind (see review by Shu *et al.*, 2000) should become collimated in this picture. On the other hand, less centrally (radially) concentrated magnetic configurations such as the potential configuration of Ouyed and Pudritz (1997a, OPI) and BP82 should collimate to cylinders.

This result also explains the range of collimation that is observed for molecular outflows. Models for observed outflows fall into two general categories: the jet-driven bow shock picture, and a wind-driven shell picture in which the molecular gas is driven by an underlying wide-angle wind component such as given by the X-wind (see review by Cabrit *et al.*, 1997). A survey of molecular outflows by Lee *et al.* (2000) found that both mechanisms are needed in order to explain the full set of systems observed.

Finally, we note that apart from these general theorems on collimation, Spruit *et al.* (1997) has proposed that a sufficiently strong poloidal field that is external to the flow could also force its collimation. According to this criterion, such a poloidal field could collimate jets provided that the field strength decreases no slower than $B_p \sim r^{-\mu}$ with $\mu \leq 1.3$.

3. SIMULATIONS: DISKS AS JET ENGINES

Computational approaches are necessary if we are to open up and explore the vast spaces of solutions to the highly nonlinear jet problem. The first simulations of non-steady MHD jets from accretion disks were performed by *Uchida and Shibata* (1985) and *Shibata and Uchida* (1986). These early simulations were based on initial states that were violently out of equilibrium and demonstrated the role of magnetic fields in launching and accelerating jets to velocities of order of the Keplerian velocity of the disk.

The published simulations of non-radiative ideal MHD YSO jets differ in their assumed initial conditions, such as the magnetic field distribution on the disk, the conditions in the plasma above the disk surfaces, the state of the initial disk corona, and the handling of the gravity of the central star. Nevertheless, they share common goals: to establish and verify the four important stages in jet evolution, namely, (i) ejection; (ii) acceleration; (iii) collimation; and (iv) stability. In the following, we describe a basic physical approach for setting up clean numerical simulations and how this leads to advances in our understanding of disk winds and outflows.

3.1. 2-Dimensional Simulations

The simulations we discuss here have been studied in greater detail in *Ouyed and Pudritz* (1997a; OPI); *Ouyed and Pudritz* (1997b; OPII); *Ouyed et al.* (1997; OPS); *Ouyed and Pudritz* (1999; OPIII); and PRO. We use these for pedagogical purposes in this review. To see animations of the simulations presented here as well as those performed by other authors, the interested reader is directed to the “animations” link at “<http://www.capca.ucalgary.ca>” (hereafter CAPCA). These simulations were run using the ZEUS (2-D, 3-D and MP) code which is arguably the best documented and utilized MHD code in the literature (*Stone and Norman*, 1992, 1994). It is an explicit, finite difference code that runs on a staggered grid. The equations generally solved are those of ideal MHD listed in Section 1, equations (2)–(6).

The evolution of the magnetic field (induction equation (4) above) is followed by the method of constrained transport. In this approach, if $\nabla \cdot \mathbf{B} = 0$ holds for the initial magnetic configuration, then it remains so for all later times to machine accuracy. The obvious way of securing this condition is to use an initial vector potential $\mathbf{A}(\mathbf{r}, \mathbf{z}, t = 0)$ that describes the desired initial magnetic field at every point in the computational domain.

To ensure a stable initial state that allows for a tractable simulation, three simple rules are useful (OPS and OPI): (i) use a corona that is in hydrostatic balance with the central object (to ensure a perfectly stable hydrostatic equilibrium of the corona, the point-mass gravitational potential should be relocated to zone centers - see Section 4.2 in OPI for details); (ii) put the disk in pressure balance with the corona above it, and (iii) use a force-free magnetic field configuration to thread the disk and corona. The initial magnetic

configurations should be chosen so that no Lorentz force is exerted on the initial (non-rotating) hydrostatic corona described above.

The BP82 self-similar solution for jets uses a simple polytropic equation of state, with an index $\gamma = 5/3$. Their solution is possible because this choice eliminates the many complications that arise from the the energy equation, while preserving the essence of the outflow problem. This Ansatz corresponds to situations where the combined effects of heating and cooling simulates a tendency toward a locally constant entropy. This choice also greatly simplifies the numerical setup and allows one to test the code against analytic solutions.

Another key simplification in this approach is to examine the physics of the outflow for fixed physical conditions in the accretion disk. Thus, the accretion disk at the base of the corona – and in pressure balance with the overlying atmosphere – is given a density profile that it maintains at all times in the simulation, since the disk boundary conditions are applied to the “ghost zones” and are not part of the computational domain. In part, this simplification may be justified by the fact that typically, accretion disks will evolve on longer time scales than their associated jets.

The hydrostatic state one arrives at has a simple analytic solution which was used as the initial state for all of our simulations and was adopted and further developed by several groups. These studies include e.g. low plasma- β monopole-like field distributions (*Romanova et al.*, 1997); a magneto-gravitational switch mechanism (*Meier et al.*, 1997); the disk accretion-ejection process (*Kudoh et al.*, 1998); the interrelation between the grid shape and the degree of flow collimation (*Ustyugova et al.*, 1998); a self-adjusting disk magnetic field inclination (*Krasnopol'sky et al.*, 1999, 2003); the interrelation between the jet's turbulent magnetic diffusivity and collimation (*Fendt and Čemeljić*, 2002); a variation of the disk rotation profile (*Vitorino et al.*, 2002); or dynamo maintained disk magnetic fields (*von Rekowski and Brandenburg*, 2004). More elaborate setups wherein the initial magnetic field configuration originates on the surface of a star and connects with the disk have also been examined (Section 5 – e.g., *Hayashi et al.*, 1996; *Goodson et al.*, 1997; *Fendt and Elstner*, 1999; *Keppens and Goedbloed*, 2000).

The lesson from these varied simulations seems to be that all roads lead to a disk field. Thus, the twisting of a closed magnetic field that initially threads the disk beyond the co-rotation radius rapidly inflates the field and then disconnects it from the star, thereby producing an open disk-field line. Likewise, simulations including dynamo generated fields in the disk lead to a state that resembles our initial setup (see Section 4). Thus, from the numerical point of view, a “fixed-disk” simulation is general and useful.

The setup requires five physical quantities to be specified at all points of the disk surface at all times (see OPI for all details). These are the disk density $\rho(r_0)$; components of the vertical and toroidal magnetic field, $B_z(r_0)$ and $B_\phi(r_0)$; and velocity components in the disk, $v_z(r_0)$

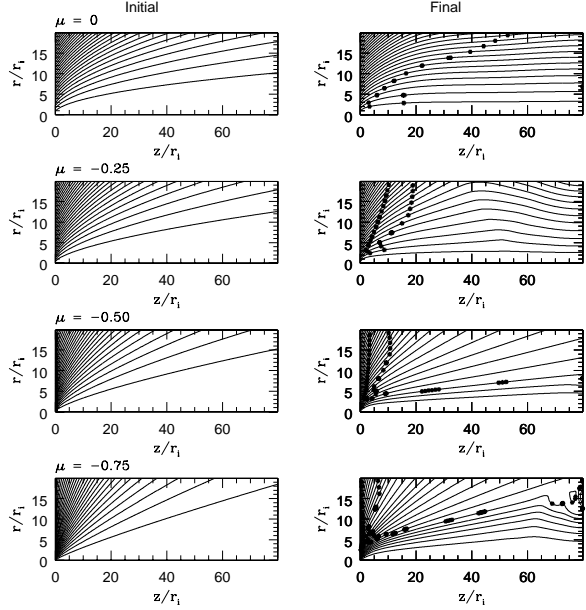


Fig. 1.— Left panels: initial magnetic field configurations for winds with $\mu = 0$ (OPI), $\mu = -0.25$ (BP), $\mu = -0.5$ (PP), and $\mu = -0.75$ (steep) Right panels: final magnetic field configurations (at $t = 400$) for each case, with Alfvén points (filled circles) and fast magneto-sonic points (stars) marked. Note the more open magnetic – and streamline – structures as μ goes down. [Adapted from PRO].

and $v_\phi(r_0)$, where r_0 is the radius (cylindrical coordinates are adopted with the disk located at $z = 0$; $r_0 = r(z = 0)$). The remaining field component $B_r(r_0)$ is determined by the solenoidal condition, while the radial inflow speed through the disk is neglected ($v_r(r_0) \simeq 0$) since it is far smaller than the sound speed in a real disk. The model is described by five parameters defined at the inner disk radius r_i , three of which describe the initial corona. The two additional parameters describe the disk physics and are ν_i , which scales the toroidal field in the disk $B_\phi = \nu_i \times (r_i/r_0)$, and the (subsonic) injection speed of material from the disk into the base of the corona, $v_{\text{inj}} = v_z(r_0)/v_\phi(r_0) \simeq 0.001$. Simulations were typically run with (500×200) spatial zones to resolve a physical region of $(80r_i \times 20r_i)$ in the z and r directions, respectively. A resolution of 10 zones per r_i provides enough dynamical range to accurately follow the smooth acceleration above the disk surface. The simulations were run up to $400t_i$ (where t_i is the Kepler time for an orbit at the inner edge of the disk).

A series of magnetic configurations is shown in Fig. 1 where the disk field is modeled as $B_z(r_0, 0) \propto r_0^{\mu-1}$. The initial configurations range from the rather well collimated (such as the potential configuration of OP97, $\mu = 0.0$; and the Blandford- Payne configuration, $\mu = -0.25$), to the initially more open configurations of Pelletier-Pudritz (PP92; $\mu = -0.5$), and steeper ($\mu = -0.75$).

A good example of a configuration that evolves into a

stationary jet was studied by OPI and is shown in the upper panel of Fig. 1). The simulation shows the existence of an acceleration region very close to the disk surface. The acceleration from the disk occurs by a centrifugal effect whereby, at some point along sufficiently inclined field lines, centrifugal force dominates gravity and gas is flung away like beads on a wire. Thus, a toroidal field component is created because the field lines corotate with the underlying disk. The inertia of the matter in the flow region ultimately forces the field to fall behind the rotation of the disk, which produces the toroidal field component. More precisely, beyond the Alfvén surface (shown as dots in the right hand panels in Fig. 1), the hoop stress induced by the self-generated B_ϕ eventually dominates, which provides the collimation. The ratio of the toroidal to poloidal magnetic field along illustrative field lines (e.g., Figs. 3 in OPS) clearly shows that the predominant magnetic field in jets beyond their fast magnetosonic (FM) surfaces is the toroidal field component. The gas is eventually collimated into cylinders parallel to the disk's axis starting at the Alfvén surface to distances much beyond the FM surface (see Fig. 1).

The final velocities achieved by such winds are of the order of 2 times the Kepler velocity, along a given field line (e.g., Fig. 3 in OPS), which translates to roughly $100\text{-}300 \text{ km s}^{-1}$ for a standard YSO. The general trend is that the jet solutions, dominated mainly by the poloidal kinetic energy, are very efficient in magnetically extracting angular momentum and energy from the disk, as confirmed by simulations performed by other groups. In 1000 years, for example, and for a standard YSO, the simulations imply that the disk winds can carry a total energy of 3×10^{43} ergs, sufficient to produce the observed molecular outflows

In OPII an initial vertical field configuration, was used. The simulations show that the strong toroidal magnetic field generated recollimates the flow towards the disk's axis and, through MHD shocks, produces knots. The knot generator is located at a distance of about $z \simeq 8r_i$ from the surface of the disk (OPS). Knots propagate down the length of the jet at speeds less than the diffuse component of the outflow. The knots are episodic, and are intrinsic to the jet and not the accretion disk, in this calculation.

A different initial state was used by Krasnopolsky *et al.* (1999), who introduce and maintain throughout the simulation, a strong outflow on the outflow axis. Otherwise, they choose an initial disk field distribution that is the same as PP92, a mass flux density $\rho v_z \propto r_0^{3/2}$, so that $k = \text{const.}$. The values of B_r and B_ϕ at the disk surface were not fixed in their simulations. (This does not guarantee that the disk or the boundary at the base will remain Keplerian over time). The fixed $B_\phi \propto r_0^{-1}$ profile adopted in the OP setup ensures exactly that - see the discussion around Eq (3.46) in OPI). To evade the problems with the initial setup mentioned above, these authors continuously launch a cylindrical wind on the axis. This imposed jet introduces currents which could significantly affect the stability and collimation of the disk wind. Their disk mass loading would predict that the disk wind should not be well collimated (see

Section 2.4), whereas their simulation does appear to collimate. This suggests that their on-axis jet may be playing a significant role in the simulation results.

3.2. The role of mass loading

The mass-load k , defined in equation (8), can be established by varying; the coronal density profile while keeping ρv_p constant (Anderson *et al.*, 2005), the disk rotational profile since $v_p = v_{\text{inj}} v_\phi$ (e.g., Vitorino *et al.*, 2002), the distribution of the poloidal magnetic field on the disk (PRO), or the distribution of both the disk magnetic field and the mass flow profile (Fendt, 2005).

The prediction that the mass load determines the collimation of the jet was tested in simulations by PRO. Fig. 1 shows that simulations with $\mu = 0, -0.25$ collimate into cylinders, while the $\mu = -0.5$ case (PP92) transitions towards the wide angle flow seen in the $\mu = -0.75$ simulation. These results confirm the theory laid out in Section 2.4. We also note that each of the simulations mentioned above results in a unique rotation profile of the jet that might in principle be observable. Going from the potential case to the Pelletier-Pudritz configuration, the radial profiles of the rotational velocity of the jets scale as power laws

$$v_\phi(r, \infty) \propto r^a \quad (18)$$

where $a = -0.76; -0.66; -0.46$ respectively. The observation of a rotational profile would help pick out a unique mass loading in this model (PRO).

The mass loading also affects the time-dependent behaviour of jets. As the mass load is varied a transition from stationary, to periodic and sometimes to a discontinuous dying jet occurs. For example, in some of the simulations it was found that low mass loads for jets lead to rapid, episodic behaviour while more heavily mass-loaded systems tend to achieve stationary outflow configurations (see OPIII).

It is interesting that the simulations of Anderson *et al.* (2005) did not find any non-steady behavior for low mass loading (differently defined than equation (8)) but instead find an instability for high mass loading. They suggest that the origin of the non-steady behavior for high mass loading is that the initially dominant toroidal field they impose could be subject to the kink instability (e.g., Cao and Spruit, 1994). The very large mass-loads, and large injection speeds ($v_{\text{inj}} = (0.01, 0.1)$) they use drive an instability probably related to excessive magnetic braking. Some of the main differences with OP are: (i) the use of the non-equilibrium set up of Krasnopol'sky *et al.* which introduces a strong current along the axis that could strongly affect the stability properties of these outflows; and (ii) the large injection speeds make the sonic surface too close to the disk (the condition that $c_s \ll v_K$ is not satisfied) and does not provide enough dynamical range for the gas launched from the disk to evolve smoothly. Numerical instabilities reminiscent of what was found by Anderson *et al.* (2005) were observed by OP and these often disappear with high enough

resolution (i.e. dynamical range). We suspect that this type of instability will disappear when a proper disk is included in the simulations (e.g., Casse and Keppens, 2002).

3.3. 3-Dimensional simulations

The stability of jets is one of the principal remaining challenges in the theory. It is well known that the purely toroidal field configurations that are used to help confine static, 3-D, tokamak plasmas are unstable (e.g., Roberts, 1967; Bateman, 1980). The resulting kink, or helical ($m = 1$) mode instability derived from a 3-D linear stability analysis is powered by the free energy in the toroidal field, namely $B_\phi^2/8\pi$ (Eichler, 1993). Why are real 3-D jets so stable over great distances in spite of the fact that they are probably threaded by strong toroidal fields?

The 3D simulations needed to investigate the importance of kink modes are still rare. Early attempts include Lucek and Bell (1996) and Hardee and Rosen (1999; see also references therein) who performed 3-D simulations of “equilibrium” jets, and found that these uniform, magnetized jet models remain Kelvin-Helmholtz (K-H) stable to low-order, surface helical and elliptical modes ($m = 1, 2$), provided that jets are on average sub-Alfvénic. This is in accord with the prediction of linear stability analysis. However, most configurations for jet simulations use rather *ad hoc* prescriptions for the initial toroidal field configuration so that it is difficult to assess how pertinent the results are to the case of a jet that establishes its own toroidal field as the jet is accelerated from the accretion disk. In general, the available analytic and numerical results for the stability of simple jets show that the fastest growing modes are of K-H type. These K-H instabilities are increasingly stabilized for super-Alfvénic jets, as M_{FM} is increased much beyond unity. It is also generally known that sub-Alfvénic jets are stable. Taken together, these results suggest that 3-D jets are the most prone to K-H instabilities a bit beyond their Alfvén surface, a region wherein their destabilizing super-Alfvénic character cannot yet be offset by the stabilizing effects engendered at large super FM numbers.

There have, as yet, only been a few attempts to simulate 3D disk winds. Contrary to what may be intuitive, it is inadvisable to perform these 3-D simulations in cylindrical coordinates. For one thing, special treatment must be given to the “wedge zones” that abut the z -axis (no longer a symmetry axis in 3D), and velocities that pass through the z -axis pose a very difficult numerical problem. Secondly, even with such technical details in hand, plane waves are badly disrupted on passing through the z -axis, and this provides an undesirable bias to what should be an unbiased (no axis should be preferred over another) 3D calculation. Fortunately, using Cartesian coordinates to simulate cylinders is feasible with careful setups as has been demonstrated in Ouyed *et al.* (2003; OCP); and Ouyed (2003). These authors used a 3D version of the OPI setup.

The central result of this study is that jets survive the threatening non-axisymmetric kink ($m = 1$) mode. The

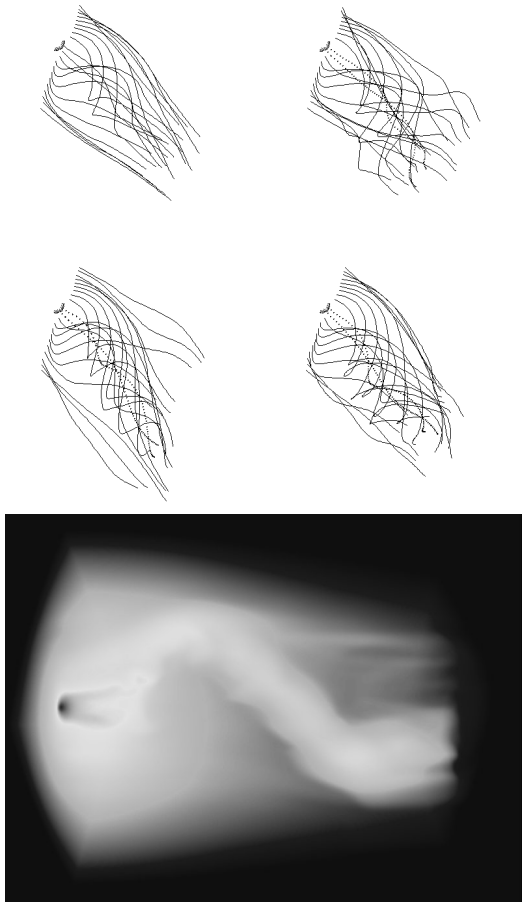


Fig. 2.— Cylindrical Jets – upper panels show snapshots of 20 magnetic field lines of the 3D simulations performed in OCP, ** at $t = 50, 130, 210$, and 240 . The two central magnetic field lines (dotted lines) originate on the central compact object (illustrated by the semi-sphere to the left). The disk axis is along the diagonal of the frame (on a 45° angle). Notice the violent jet behavior in the in-between frames when the kink mode appears. The jet eventually aligns itself with the original disk's axis acquiring a cylindrically collimated shape. Corkscrew Jets – The lower panel is a map of the jet column density at $t = 320$ for a simulation with a v_ϕ profile, imposed at the accretion disk, that is different from the simulation shown in the upper four panels (see OCP). The jet has settled into a quasi-steady state structure in the shape of a “corkscrew” (colors arranged from blue to red to represent low and high values of the density). The disk (not visible) is on the left-hand side of the image, and outflow is from left to right. [Adapted from OCP].

simulated jets maintain their long-term stability through a self-limiting process wherein the average Alfvénic Mach number within the jet is maintained to order unity. This is accomplished in at least two ways: (i) poloidal magnetic field is concentrated along the central axis of the jet forming a “backbone” in which the Alfvén speed is sufficiently high to reduce the average jet Alfvénic Mach number to unity, and (ii) the onset of higher order Kelvin-Helmholtz “flute” modes ($m \geq 2$) reduce the efficiency with which

the jet material is accelerated, and transfer kinetic energy of the outflow into the stretched, poloidal field lines of the distorted jet. This too has the effect of increasing the Alfvén speed, and thus reducing the Alfvénic Mach number. The jet is able to survive the onset of the more destructive $m = 1$ mode in this way. It was further discovered that jets go into alternating periods of low and high activity as the disappearance of unstable modes in the sub-Alfvénic regime enables another cycle of acceleration to super-Alfvénic speeds. The period of the episodic (low vs. high) behavior uncovered in the case of the wobbling jet (upper four panels in Fig. 2) is of the order of $200 t_i$. For a typical young stellar object of mass $0.5M_\odot$ and for $r_i \sim 0.05$ AU (i.e. $t_i \sim 0.9$ day), this would correspond to a minimum period of roughly 180 days. This is consistent with the temporal variations of the observed YSOs outflow velocities which appears to occur on timescales of a few years (Woitas *et al.*, 2002).

Jets ultimately settle into relatively stable end-states involving either corkscrew (lower panel in Fig. 2), or wobbling types of structure (upper four panels in Fig. 2). The difference in the two type of jets can be traced to the difference in the v_ϕ profiles imposed at the accretion disk (see OCP for more details). This trend has been uncovered in 3D simulations of large scale jets where wiggled jets have also been observed after the jets survived the destructive era (Uchida *et al.*, 1992; Todo *et al.*, 1993; Nakamura *et al.*, 2001; Nakamura and Meier, 2004). For completeness, we should mention the recent similar simulations performed by Kigure and Shibata (2005) which included the disk self-consistently. These studies also show that non-axisymmetric perturbations dominate the dynamics. However, these simulations were only run for very short times, never exceeding 2 inner-disk orbital periods due to numerical obstacles reported by the authors. In OCP simulations, it was shown that the Cartesian grid (also used by Kigure and Shibata) induces artificial modes in the early stages of the simulations and only after many orbital periods that these become washed out before the real modes enter the dynamics. Another suggested end-state for 3D jets is a minimum-energy “Taylor state”, wherein the jet maintains comparable poloidal and toroidal field components (Königl and Choudhuri, 1985). This alternative does not pertain to our simplified simulations since we do not allow for internal magnetic energy dissipation.

In summary, a large body of different simulations have converged to show that jets; (i) are centrifugally disk winds; (ii) are collimated by the “hoop stress” engendered by their toroidal fields; (iii) achieve two types of configuration depending on the mass loading that takes place in the underlying accretion disc – those that achieve collimation towards a cylinder, and those that have a wide-angle structure; (iv) achieve two types of regimes depending on the mass loading that takes place in the underlying accretion disc – those that achieve a stationary state, and those that are episodic; (v) achieve stability by a combination of MHD mode coupling and “back-bone” effect leading to a self-regulating mechanism which saturates the instabilities; and

(vi) achieve different morphologies ranging from cylindrical wobbling to cork-screw structure, depending on the profile of v_ϕ imposed on the underlying accretion disk.

4. COUPLED DISK-JET EVOLUTION

While it is physically useful to regard the accretion disk as a boundary condition for the jet, this ignores critical issues such as the self-consistent radial distribution of the mass loading, or of the threading magnetic field across the disk. These, and other degrees of freedom can be found by solving the combined disk-outflow problem, to which we now turn.

Significant progress on the launch of disk winds has been made by theoretical studies of a restricted class of self-similar 2D models (e.g. *Wardle and Königl*, 1993; *Li*, 1995, 1996; *Ferreira*, 1997; *Casse and Ferreira*, 2000). Since centrifugally driven outflows can occur for completely cold winds (BP82), the models have examined both “cold” and “warm” (i.e., with some kind of corona) conditions. In the former class, material from some height above the disk mid-plane must move upwards and eventually be accelerated outwards in a jet. Therefore, there must be a direct link between the physics of magnetized disks, and the origin of outflows.

Calculations show that in order to match the properties of jets measured by *Bacciotti et al.* (2000), warm wind solutions are preferred, wherein a disk corona plays a central role. In this situation, gas pressure imbalance will assist with feeding the jet. A warm disk corona is expected on general grounds because it is a consequence of the magneto-rotational instability (MRI), as the vertically resolved disk simulations of *Miller and Stone* (2000) have shown.

A semi-analytic model of the radial and vertical disk structure, that includes self-consistently the outflow, has also been presented by *Campbell* (2003). These solutions demonstrate explicitly that the outflow contributes to the loss of angular momentum in the disk by channeling it along field lines into the outflow. For self-consistent solutions to be possible, the turbulent Mach number has to be between 0.01 and 0.1.

Models of outflows and jets generally assume ideal (non-resistive) MHD. However, inside the disk non-ideal effects must become important, because the accreting matter would otherwise never be able to get onto the field lines that thread the disk and connect it with the outflow. In recent two-dimensional models, *Casse and Keppens* (2002, 2004) assumed a resistivity profile, analogously to the Shakura and Sunyaev prescription. This assumes the presence of an underlying turbulence within the disk. Only fairly large values of the corresponding α_{SS} parameter of around 0.1 have been used. The subscript SS refers to *Shakura and Sunyaev* (1973), who were the first to introduce this viscosity parameter. In all cases the system evolves to a steady equilibrium. Using resistive simulations in a different context, *Kuwabara et al.* (2005) demonstrated that a substantial amount of energy can be transported by Poynting flux if the poloidal

field falls off with distance no faster than r^{-2} . Otherwise, the fast magnetosonic point is located closer to the Alfvén point and the jet will be dominated by kinetic energy, which is the case in the simulations of *Casse and Keppens* (2004).

The general stability of disk-outflow solutions is still being debated and the result may depend on the detailed assumptions about the model. In the solutions discussed here the accretion stress comes entirely from the large scale magnetic field rather than some small scale turbulence. As emphasized by *Ferreira and Casse* (2004), real disks have a turbulent viscosity just as they have turbulent magnetic diffusivity or resistivity. However, if the accretion stress does come entirely from the large scale magnetic field, the wind-driven accretion flows may be unstable (*Lubow et al.*, 1994). *Königl* (2004) has shown recently that there are in fact two distinct solution branches—a stable and an unstable one. He argues that real disk/wind systems would correspond to the stable branch.

Finally, the idea of a gently flared accretion disk is likely to be merely the result of the modeler’s simplification rather than observational reality. Indeed, accretion disks can be warped due to various instabilities which can be driven by radiation from the central object (e.g., *Pringle*, 1996), or, more likely, by the outflow itself (*Schandl and Meyer*, 1994). If a system is observed nearly edge-on, a warp in the accretion disk produces periodic modulations of the light curve. As *Pinte and Ménard* (2004) have demonstrated, this may be the case in AA Tau. Observations frequently reveal major asymmetries in bipolar outflows, which may be traced back to the corresponding asymmetries in the disk itself. The possible causes for these asymmetries may be either an externally imposed asymmetry such as one-sided heating by a nearby OB association, or an internal symmetry breaking of the disk-wind solution as a result increased rotation. Examples of the latter are familiar from the study of mean field dynamo solutions of accretion disks (*Torkelson and Brandenburg*, 1994).

4.1. Dead zones

So far it has been assumed that the magnetic field is well coupled to the disk. This is certainly valid for most of the envelope of an accretion disk, which is ionized by a combination of cosmic rays, as well as X-rays from the central YSO. However, the deeper layers of the disk are strongly shielded from these ionizing agents and the degree of ionization plummets.

This dense layer, which encompasses the bulk of the disk’s column density, cannot maintain a sufficiently high electron fraction, and is referred to as the dead zone (*Gammie*, 1996). It is the poorly ionized region within which the MRI fails to grow as a consequence of the diffusivity of the field. Recent work of *Fleming and Stone* (2003) shows that, although the local Maxwell stress drops to negligible values in the dead zones, the Reynolds stress remains approximately independent of height and never drops below approximately 10% of the maximum Maxwell stress, pro-

vided the column density in that zone is less than 10 times the column of the active layers. The non-dimensional ratio of stress to gas pressure is just the viscosity parameter, α_{SS} . *Fleming and Stone* (2003) find typical values of a few times 10^{-4} in the dead zones and a few times 10^{-3} in the MRI-active layers. *Inutsuka and Sano* (2005) have questioned the very existence of dead zones, and proposed that the turbulent dissipation in the disk provides sufficient energy for the ionization. On the other hand, their calculation assumes a magnetic Reynolds number that is much smaller than expected from the simulations (see *Matsumura and Pudritz*, 2006; MP06).

The radial extent of the dead zone depends primarily upon the disk column density as well as effects of grains and radiation chemistry (e.g., *Sano et al.*, 2000; *Matsumura and Pudritz*, 2005, MP05; and MP06). Inside the dead zone the magnetic Reynolds number tends to be below a certain critical value that is somewhere between 1 and 100 (*Sano and Stone*, 2002), making MRI-driven turbulence impossible. Estimates for the radial extent of the dead zone range from 0.7–100 AU (*Fromang et al.*, 2002), to 2–20 AU in calculations by *Semenov et al.* (2004). For *Chiang et al.* (2001) models of disks that are well constrained by the observations, and whose surface density declines as $\Sigma \propto r_0^{-3/2}$, MP05 find that the extent of the dead zone is robust – extending out to 15 AU typically, and is fairly independent of the ionizing environment of the disk.

For smaller radii, thermal and UV ionization are mainly responsible for sustaining some degree of ionization. The significance of the reduced value of α_{SS} in the dead zones is that it provides a mechanism for stopping the inward migration of Jupiter-sized planets (MP05, MP06). Jets can still be launched from the well-coupled surface layer above the dead zone (e.g., *Li*, 1996; *Campbell*, 2000).

When the MRI is inactive in the body of the disk, alternative mechanisms of angular momentum transport are still possible. In protostellar disks there are probably at least two other mechanisms that might contribute to the accretion torque: density waves (*Rózyczka and Spruit*, 1993), and the interaction with other planets in the disk (*Goodman and Rafikov*, 2001).

A more controversial alternative is to drive turbulence by a nonlinear finite amplitude instability (*Chagelishvili et al.*, 2003). While *Hawley et al.* (1999) have given general arguments against this possibility, *Afshordi et al.* (2005) and other groups have continued investigating the so-called bypass to turbulence. The basic idea is that successive strong transients can maintain a turbulent state in a continuously excited manner. *Lesur and Longaretti* (2005) have recently been able to quantify more precisely the critical Reynolds number required for instability. They have also highlighted the importance of pressure fluctuations that demonstrate that the general argument by *Balbus et al.* (1996) is insufficient.

Finally, the role of vertical (convectively stable) density stratification in disks and the possibility of the so-called

strato-rotational instability has been proposed as a possible mechanism for disk turbulence (*Dubrulle et al.*, 2005). This instability was recently discovered by *Molemaker et al.* (2001) and the linear stability regime was analyzed by *Shalybkov and Rüdiger* (2005). However, the presence of no-slip radial boundary conditions that are relevant to experiments and used in simulations are vital. Indeed, the instability vanishes for an unbounded regime, making it irrelevant for accretion disks (*Umurhan*, 2006).

4.2. Advection vs. dynamo generated magnetic fields

One of the central unresolved issues in disk wind theory is the origin of the threading magnetic field. Is it dragged in by the gravitational collapse of an original magnetized core, or is it generated *in situ* by a disk-dynamo of some sort?

The recent direct detection of a rather strong, true disk field of strength 1 kG at 0.05 AU in FU Ori, provides new and strong support for the disk wind mechanism (*Donati et al.* 2005). The observation technique uses high-efficiency high-resolution spectropolarimetry and holds much promise for further measurements. This work provides excellent evidence that distinct fields exist in disks in spite of processes such as ambipolar diffusion which might be expected to reduce them.

4.2.1 Turbulence effects. Accretion disks are turbulent in the well-coupled lower corona and beyond. They are also intrinsically three-dimensional and unsteady. Questions regarding the stability of disks concern therefore only the mean (azimuthally averaged) state, where all turbulent eddies are averaged out. The averaged equations used to obtain such solutions incorporate a turbulent viscosity. In this connection we must explain that the transition from a macroscopic viscosity to a turbulent one is more than just a change in coefficients, because one is really entering a new level of description that is uncertain in many respects. For example, in the related problem of magnetic diffusion it has been suggested that in MRI-driven turbulence, the functional form of turbulent magnetic diffusion may be different, such that it operates mainly on the system scale and less efficiently on smaller scales (*Brandenburg and Sokoloff*, 2002). It is therefore important to use direct simulations to investigate the stability in systems that might be unstable according to a mean field description. There is no good example relevant to protostellar disks, but related experience with radiatively dominated accretion disks, where it was found that the so-called Lightman–Eardly instability might not lead to the breakup of the disk (*Turner et al.*, 2004), should provide enough reason to treat the mean-field stability problem of protostellar disks with caution. Also, one cannot exclude that circulation patterns found in simulations of the two-dimensional mean-field equations (e.g., *Kley and Lin*, 1992) may take a different form if the fully turbulent three-dimensional problem was solved.

The turbulent regions of disks will generally be capable of dynamo action – wherein an ordered field is generated by feeding on the energy that sustains the turbulence. These

two aspects are in principle interlinked, as has been demonstrated some time ago using local shearing box simulations. These simulations show not only that the magnetic field is generated from the turbulence by dynamo action, but also that the turbulence itself is a consequence of the magnetic field via the MRI (Brandenburg *et al.*, 1995; Stone *et al.*, 1996).

In comparing numerical dynamos with observational reality, it is important to distinguish between two different types of dynamos: small scale and large scale dynamos (referring primarily to the typical physical scale of the field). Both types of dynamos have in general a turbulent component, but large scale dynamos have an additional component on a scale that is larger than the typical scale of the turbulence. Physically, this can be caused by the effects of anisotropies, helicity, and/or shear. These large scale dynamos are amenable to mean field modeling (see below). Small scale dynamos, on the other hand, tend to be quite prominent in simulations, but they are not described by mean field models. However, small scale dynamos could be an artefact of using unrealistically large magnetic Prandtl numbers in the simulations. Protostellar disks have magnetic Prandtl numbers, ν/η , around 10^{-8} , so the viscosity of the gas, ν , is much smaller than the diffusivity of the field, η ; see Table 1 of Brandenburg and Subramanian (2005). High magnetic Prandtl numbers imply that the field is advected with the flow without slipping too much, whereas for low numbers the field readily slips significantly with respect to the flow. At the resistive scale, where the small scale dynamo would operate fastest, the velocity is still in its inertial range where the spatial variation of the velocity is much rougher than for unit magnetic Prandtl number (Boldyrev and Cattaneo, 2004). This tends to inhibit small scale dynamo action (Schekochihin *et al.*, 2005). In many simulations, especially when a subgrid scale prescription is used, the magnetic Prandtl number is effectively close to unity. As a consequence, the production of small scale field may be exaggerated. It is therefore possible that in real disks large scale dynamo action is much more prominent than what is currently seen in simulations.

In mean field models, only the large scale field is modeled. In addition to a turbulent magnetic diffusivity that emerges analogously to the turbulent viscosity mentioned above, there are also non-diffusive contributions such as the so-called α effect wherein the mean electromotive force can acquire a component parallel to the mean field, $\alpha_{\text{dyn}} \bar{B}$; see Brandenburg and Subramanian (2005) for a recent review. For symmetry reasons, α_{dyn} has on average opposite signs above and below the midplane. Simulations of Ziegler and Rüdiger (2000) confirm the unconventional negative sign of α_{dyn} in the upper disk plane, which was originally found in Brandenburg *et al.* (1995). This has implications for the expected field parity which is expected to be dipolar (anti-symmetric about the midplane); see Campbell *et al.* (1998) and Bardou *et al.* (2001). Although a tendency toward dipolar fields is now seen in some global accretion disk simulations (De Villiers *et al.*, 2005), this issue cannot as yet be

regarded as conclusive.

4.2.2 Outflows from dynamo-active disks. Given that the disk is capable of dynamo action, what are the relative roles played by ambient and dynamo-generated fields? This question has so far only been studied in limiting cases. The first global simulations were axisymmetric, in which case dynamo action is impossible by the Cowling (1934) theorem. Nevertheless, such simulations have demonstrated quite convincingly that a jet can be launched by winding up the ambient field and driving thereby a torsional Alfvén wave (Matsumoto *et al.*, 1996). These simulations are scale invariant and, although they were originally discussed in the context of active galaxies, after appropriate rescaling, the same physics applies also to stellar disk outflows.

When the first three-dimensional simulations became available an immediate issue was the demonstration that MRI and dynamo action are still possible (Hawley, 2000). Although the simulations were applied to model black hole accretion disks, many aspects of such models are sufficiently generic that they carry over to protostellar disks as well. These simulations showed that the dynamo works efficiently and produces normalized accretion stresses ($\alpha_{\text{SS}} \approx 0.1$) that exceed those from local simulations ($\alpha_{\text{SS}} \approx 0.01$). The global simulations did not at first seem to show any signs of outflows, but this was mainly a matter of looking at suitable diagnostics, which emphasizes the tenuous outflows rather than the much denser disk dynamics (De Villiers *et al.*, 2005). Although these simulations have no ambient field, a large scale field develops in the outflow region away from the midplane. However, it is difficult to run such global simulations for long enough to exclude a dependence of the large scale field on the initial conditions. The outflows are found to be uncollimated such that most of the mass flux occurs in a conical shell with half-opening angle of 25–30° (De Villiers *et al.*, 2005).

These very same properties are also shared by mean field simulations, where the three-dimensional turbulent dynamics is modeled using axisymmetric models (von Rekowski *et al.*, 2003). In these simulations (Fig. 3), where the field is entirely dynamo-generated, there is an uncollimated outflow with most of the mass flux occurring in a conical shell with a half-opening angle of about 25–30°, just like in the three-dimensional black hole simulations. The field strength generated by dynamo action in the disk is found to scale as $B_p \propto r^{-2}$. This is very similar to the scaling for poloidal field strength found in collapse simulations (see Banerjee and Pudritz, 2006).

The conical outflows discussed above have tentatively been compared with the observed conical outflows inferred for the BN/KL region in the Orion nebula out to a distance of 25–60 AU from its origin (Greenhill *et al.*, 1998). One may wonder whether collimated outflows are only possible when there is an ambient field (see Section 3). This conclusion might be consistent with observations of the Taurus-Auriga molecular cloud. Ménard and Duchêne (2004) found that, although T Tauri stars are oriented randomly with respect to the ambient field, there are no bright and ex-

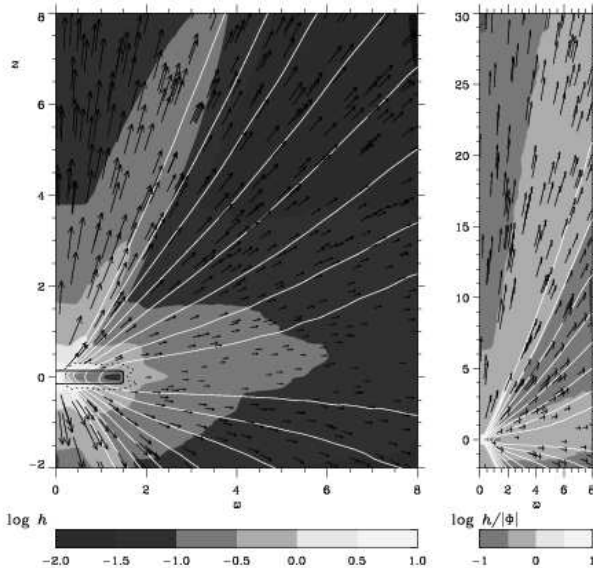


Fig. 3.— Outflow from a dynamo active accretion disk driven by a combination of pressure driving and magneto-centrifugal acceleration. The extent of the domain is $[0, 8] \times [-2, 30]$ in nondimensional units (corresponding to about $[0, 0.8]$ AU \times $[-0.2, 3]$ AU in dimensional units). Left panel: velocity vectors, poloidal magnetic field lines and gray scale representation of the specific enthalpy h in the inner part of the domain. Right panel: velocity vectors, poloidal magnetic field lines and normalized specific enthalpy $h/|\Phi|$ in the full domain. [Adapted from *von Rekowski et al. (2003)*].

tended outflows when the axis is perpendicular to the ambient field. Note that *Spruit and Uzdensky (2005)* have argued that the efficiency of dragging an ambient field toward the star have been underestimated in the past, provided the field segregates into many isolated flux bundles.

In summing up this section we note that all magnetic disk models produce outflows of some form. However, the degree of collimation may depend on the possibility of an ambient field. An important ingredient that seems to have been ignored in all combined disk-jet models is the effect of radiation. There are also many similarities between the outflows in models with and without explicitly including the disk structure. Although these simulations are non-ideal (finite viscosity and resistivity), the various Lagrangian invariants (mass loading parameter, angular velocity of magnetic field lines, as well as the angular momentum and Bernoulli constants) are still very nearly constant along field lines outside the disk.

5. JETS AND STAR-DISK INTERACTION

In this section we review the recent development concerning the interaction of young stellar magnetospheres with the surrounding accretion disk and the contribution

that these processes may have to the formation of jets.

Perhaps the most important clue that star-disk interaction is an important physical process comes from the observation that many YSOs are observed to spin at only a small fraction ($\simeq 10\%$) of their break-up speed (e.g., *Herbst et al., 2002*). They must therefore undergo a significant spin-down torque that almost cancels the strong spin-up that arises from gas accretion from the inner edge of the Keplerian disk.

Three possible spin-down torques have been proposed: (i) disk-locking – a magnetospheric connection between the disk and the star which dumps accreted angular momentum back out into the disk beyond the co-rotation radius (*Königl 1991*); (ii) an X-wind – a centrifugally driven outflow launched from the very inner edge of the accretion disk which intercepts the angular momentum destined for the star (see chapter by *Shang et al.*); and (iii) an accretion-powered stellar wind – in which the slowly rotating, central star drives a massive ($\dot{M}_{w,*} \simeq 0.1 \dot{M}_a$), stellar wind that carries off the bulk of the angular momentum as well as a fraction of the energy, that is deposited into the photosphere by magnetospheric accretion (*Matt and Pudritz, 2005b*). The last possibility implies that the central object in an accretion disk also drive an outflow, which is in addition to the disk wind. Separating the disk wind from the outflow from the central object would be difficult, but the shear layer that separates them might generate instabilities and shocks that might be diagnostics.

The strength of the star-disk coupling depends on the strength of the stellar magnetic field. Precise stellar magnetic field measurements exist for nine TTSs, while for seven other stars statistically significant fields have been found (see *Symington et al., 2005b* and references therein). Zeeman circular-polarization measurements in He I of several classical TTs give direct evidence of kG magnetic fields with strong indication of considerable field variation on the time scales of years (*Symington et al., 2005b*). For a sample of stars a magnetic field strength up to 4 kG fields could be derived (DF Tau, BP Tau), as for others, notably the jet source DG Tau, no significant field could be detected at the time of observation.

5.1. Basic processes

5.1.1 Variable accretion from a tipped dipole. A central dipolar field inclined to the rotation axis of star and disk may strongly disturb the axisymmetry of the system. Photometric and spectroscopic variability studies of AA Tau give evidence for time-dependent magnetospheric accretion on time scales of the order a month. Monte-Carlo modeling shows that the observed photo-polarimetric variability may arise by warping of the disk that is induced by a tipped magnetic dipole (*O'Sullivan et al., 2005*). More general investigations of the warping process by numerical simulations show that the warp could evolve into a steady state precessing rigidly (*Pfeiffer and Lai, 2004*). Disks can be warped by the magnetic torque that arises from the a slight misalignment

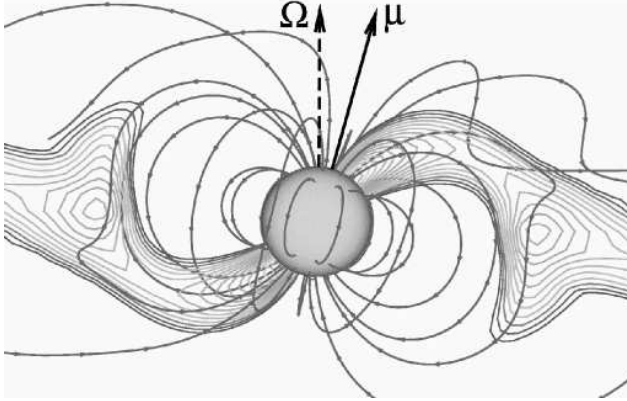


Fig. 4.— Slice through a funnel stream. Density contours from $\rho = 0.2$ to $\rho = 2.0$. The density of the disk corona is $\rho = 0.01 - 0.02$. Selected magnetic field lines. The rotational axis and the magnetic moment are indicated as Ω and μ . [Adapted from Romanova *et al.* (2004).]

ment between the disk and star's rotational axis (Lai 1999). Disk warping may also operate in the absence of a stellar magnetosphere since it can be induced by the interaction between a large-scale magnetic field that is anchored in the disk, and the disk electric current. This leads to a warping instability and to the retrograde precession of magnetic jets/outflows (Lai, 2003).

Three-dimensional radiative transfer models of the magnetospheric emission line profile based on the warped disk density and velocity distribution obtained by numerical MHD simulations give gross agreement with observations with a variability somewhat larger than observed (Symington *et al.*, 2005a).

5.1.2 Magnetic flux. Compared to the situation of a pure disk magnetic field, the magnetic field of the star may add substantial magnetic flux to the system. For a polar field strength B_0 and a stellar radius R_* , the large scale stellar dipolar field (ignoring angular variations)

$$B_{p,*}(r) \simeq 40 \text{ G} \left(\frac{B_0}{1 \text{ kG}} \right) \left(\frac{r}{3 R_*} \right)^{-3} \quad (19)$$

has to be compared to the accretion disk poloidal magnetic field which is provided either by a disk dynamo or by advection of ambient interstellar field,

$$B_{p,\text{disk}} < B_{\text{eq}}(r) = 20 \text{ G} \alpha^{-1/2} \left(\frac{\dot{M}_a}{10^{-6} M_\odot \text{ yr}^{-1}} \right)^{1/2} \cdot \left(\frac{M_*}{M_\odot} \right)^{1/4} \left(\frac{H/r}{0.1} \right)^{-1/2} \left(\frac{r}{10 R_\odot} \right)^{-5/4} \quad (20)$$

where B_{eq} is the equipartition field strength in the disk. This flux will not remain closed, but will inflate and open up as magnetic field lines are sheared and extract gravitational potential energy from the accreting flow (e.g., Uzdensky *et al.*, 2002; Matt and Pudritz, 2005a). These field lines therefore effectively become a disk field, and therefore follow

the processes of disk wind production we have already discussed.

The additional Poynting flux that threads the disk may assist the jet launching by MHD forces and may serve as an additional energy reservoir for the kinetic energy of the jet implying greater asymptotic jet speed (Michel scaling; Michel, 1969; Fendt and Camenzind, 1996).

5.1.3 Disk locking vs. stellar winds. The spin of the star will depend on how angular momentum arriving from the disk, is dealt with. In the magnetic “disk locking” picture, the threading field of the disk will re-arrange the global angular momentum budget. The torque on the star by the accretion of disk matter is

$$\tau_a = \dot{M}_a (GM_* r_{\text{in}})^{1/2} \quad (21)$$

(e.g., Matt and Pudritz, 2005a), with the disk accretion rate \dot{M}_{acc} , the stellar mass M_* and the disk inner radius r_{in} inside the corotation radius $r_{\text{co}} = (GM_*)^{1/3} \Omega_*^{-2/3}$. On the other hand if “disk locking” is present, the stellar rotation may be decelerated by the magnetic torque due to stellar field lines connecting the star with the accretion disk outside R_{co} . The differential magnetic torque acting on a disk annulus of dr width is

$$d\tau_{\text{mag}} = r^2 B_\phi B_z dr. \quad (22)$$

While B_z in principle follows from assuming a central dipolar field, the induction of toroidal magnetic fields is model dependent (disk resistivity, poloidal field structure). This is why recent numerical simulations of dipole-disk interaction that simultaneously evaluate the poloidal and toroidal field components have become extremely valuable.

If indeed the star loses angular momentum to the disk (this is not yet decided by the simulations, see below), both disk accretion and jet formation are affected. In order to continue accretion, excess angular momentum has to be removed from the accreting matter. A disk jet can be an efficient way to do this, as has been supposed in the X-wind picture.

The central stellar magnetic field may launch a strong stellar wind to rid itself of the accreted angular momentum. Such an outflow will interact with the surrounding disk wind. If true, observed YSO jets may consist of two components – the stellar wind and the disk wind, with strength depending on intrinsic (yet unknown) parameters. The stellar wind (open field lines of stellar magnetosphere) exerts a spin-down torque upon the star of magnitude

$$\dot{M}_{\text{wind},*} \Omega_* r_A^2 = 3 \times 10^{36} \frac{\text{g cm}^2}{\text{s yr}} \left(\frac{\Omega_*}{10^{-5} \text{ s}^{-1}} \right) \cdot \left(\frac{r_A}{30 R_\odot} \right)^2 \left(\frac{\dot{M}_{\text{wind},*}}{10^{-9} M_\odot \text{ yr}^{-1}} \right) \quad (23)$$

As a historical remark we note that the model topology of dipole-plus-disk field were introduced for protostellar jet formation more than 20 years ago in the MHD simulations

of *Uchida and Shibata* (1984). Further investigations considering the detailed physical processes involved in disk truncation and channeling the matter along the dipolar field lines by *Camenzind* (1990), *Königl* (1991) and *Shu et al.* (1994) resulted in a breakthrough of these ideas to the protostellar jet community.

5.2. Numerical simulations of star-disk interaction

The numerical simulation of the magnetospheric star-disk interaction is technically most demanding since one must treat a complex model geometry in combination with strong gradients in magnetic field strength, density and resistivity. In general, this may imply a large variation in physical times scales for the three components of disk, jet, and magnetosphere, which all have to be resolved numerically. Essentially, numerical modeling of the star-disk interaction requires a *diffusive and viscous MHD code including radiative transfer*. In addition, realistic models for reconnection processes and disk opacity are needed. Then, such a code has to run with *high spatial and temporal resolution* on a global scale.

Compared to the situation about a decade ago when there was still only *Uchida and Shibata*'s (1984) initial (though ten years old) simulation available, today huge progress has been made with several groups (and also codes) competing in the field. Early simulations were able to follow the evolution only for a few rotations of the inner disk (note that 100 rotations at the co-rotation radius correspond to 0.3 Keplerian rotations at 10 co-rotation radii) (*Hayashi et al.*, 1996; *Miller and Stone*, 1997; *Goodson et al.*, 1997). Among the problems involved is the initial condition of the simulation, in particular the nature of the disk model which could be numerically treated. A steady initial corona will strongly shear with the Keplerian disk leading to current sheet (thus pressure gradients) along the disk surface. If the simulations run long enough, this could be an intermittent feature. However, the danger exists that the artificial current sheet will fatally destroy the result of the simulation. Applying a Shakura-Sunyaev disk for the initial disk structure, the code should also consider α_{SS} viscosity. Otherwise the initial disk evolution is not self-consistent (see, e.g., *Goodson et al.*, 1997).

The next step is to increase the grid resolution and to redo the axisymmetric simulations. *Goodson et al.* (1999) and *Goodson and Winglee* (1999) were able to treat several hundreds of (inner) disk rotations on a global grid of 50 AU extension. The main result of these simulations is a two component flow consisting of a fast and narrow axial jet and a slow disk wind, both launched in the inner part of the disk ($r < 1$ AU). An interesting feature is that the narrow axial jet is actually a collimation in density and not in velocity. Close to the inner disk radius repetitive reconnection processes are seen on time scales of a couple of rotation periods. The dipolar field inflates and an expanding current sheet builds up. After field reconnection along the current sheet, the process starts all over again. The os-

cillatory behaviour leads to the ejection of axial knots. On average the central dipolar magnetosphere remains present and loaded with plasma. Forbidden emission line intensity maps of these simulations have been calculated and allow for direct comparison with the observations. However, the numerically derived time and length scales of axial knots were still too different from what is observed. The magnetospheric origin of jets (stellar dynamo) in favor of a pure disk origin ("primordial field") has also been stressed by *Matt et al.* (2002).

In order to be able to perform long-term simulations of dipolar magnetospheres interacting with the accretion disk, *Fendt and Elstner* (1999, 2000) neglected the evolution of the disk structure and instead assume that the disk is a fixed boundary condition for the outflow (as in OPI). After 2000 rotations a quasi-steady state was obtained with a two-component outflow from disk and star. The outflow expands almost radially without signature of collimation on the spatial scale investigated (20×20 inner disk radii). One consequence of this very long simulation is that the axial narrow jet observed in other simulations might be an intermittent feature launched in the early phase of the simulation as the initial field is reconfigured to a new equilibrium. The axial outflow in this simulations is massive but slow, but tends to develop axial instabilities for a lower mass loading. Clearly, since the disk structure was not been taken into account, nothing could be said about the launching process of the outflow out of the disk.

In a series of ideal MHD simulations Romanova and collaborators succeeded in working out a detailed and sufficiently stable numerical model of magnetospheric disk interaction. They were the first to simulate the axisymmetric funnel flow from the disk inner radius onto the stellar surface (*Romanova et al.*, 2002) on a global scale ($R_{\max} = 50R_{\text{in}}$) and for a sufficiently long period of time (300 rotations) in order to reach a steady state in the accretion funnel. The funnel flow with free-falling material builds up as a gap opens up between disk and star. The authors further investigated the angular momentum exchange due to the disk "locking" by the funnel flow. Slowly rotating stars seem to break the inner disk region and spin up, while rapid rotators would accelerate the inner disk region to super-Keplerian velocity and slow down themselves. Only for certain stellar rotational periods a "torque-less" accretion could be observed. Strong outflows have not been observed for the parameter space investigated, probably due to the matter dominated corona which does not allow for opening-up the dipolar field.

Further progress has been achieved extending these simulations to three dimensions (*Romanova et al.*, 2003, 2004). For the first time it has been possible to investigate the interaction of an inclined stellar dipolar magnetosphere with the surrounding disk. For zero inclination axisymmetric funnels are found as in the axisymmetric simulations. For non-zero inclination the accretion splits in two main streams following the closest path from the disk to the stellar surface as is seen in Fig. 4. Magnetic braking changes the disk struc-

ture in several ways – its density structure (gaps, rings), its velocity structure (sub-Keplerian region) and its geometry (warping). The slowly rotating star is spun up by accreting matter but this acceleration does only weakly depend on inclination. For completeness we should note that for these simulations a clever approach for the numerical grid has been applied, the “cubed grid” which does not obey the singular axes as for spherical coordinates.

The star-disk coupling by the stellar magnetosphere was also investigated by *Küker et al.* (2003). These simulations have been performed in axisymmetry, but an advanced disk model has been applied. Taking into account α -viscosity, a corresponding eddy magnetic diffusivity and radiative energy transport, the code enables the authors to treat a realistic *accretion* disk in their MHD simulations. As a result the simulations could be advanced to very long physical time steps into a quasi stationary state of the disk evolution. The authors show that the commonly assumed 1000 G magnetosphere is not sufficient to open up a gap in the disk. Unsteady outflows may be launched outside of the corotation radius with mass loss rates of about 10 % of the accretion rate. The authors note that they were unable to detect the narrow axial jet seen in other publications before (in agreement with *Fendt and Elstner*, 2000). Magnetic braking of the star may happen in some cases, but is overwhelmed by the accretion torque still spinning up the star (however, these simulations treat the stellar surface as inner boundary condition).

Using a different approach, the boundary condition of a stellar *dipolar* magnetosphere or a large scale disk field were relaxed. This allows for the interaction of a stellar dipole with a *dynamo*-generated disk magnetic field (*von Rekowski and Brandenburg*, 2004), or the evolution of a *dynamo*-generated stellar field affected by a surrounding disk with its own disk dynamo (*von Rekowski and Brandenburg*, 2006) to be studied. The results of this work are in agreement with previous studies, and directly prove that a disk surrounding a stellar magnetosphere may actually develop its own magnetic field strong enough to launch MHD outflows. In agreement with results by *Goodson and Winglee* (1999), accretion tends to be unsteady and alternating between connected and disconnected states. Even for realistic stellar fields of several hundred gauss the magnetic spin-down torque is insufficient to overcome the spin-up torque from the accretion flow itself. As shown by the authors, angular momentum exchange is complex and may vary in sign along the stellar surface, braking some parts of the star and accelerating others. The *dynamo*-generated stellar field may reach up to 750 G and switches in time between dipolar and quadrupolar symmetry, while the *dynamo*-generated 50 G disk field is of dipolar symmetry. In general, the *dynamo*-generated stellar field is better suited to drive a stellar wind. The simulations show that for these cases stellar wind braking is more efficient than braking by the star-disk coupling, confirming the results of *Matt and Pudritz* (2005a).

Recent studies of torque-less accretion (*Long et al.*,

2005) compare cases of a (i) weak stellar magnetic field within a dense corona and (ii) a strong field in a lower density corona. They investigate the role of quasi-periodic field line reconnection in coupling the disk and stellar fields. Unlike previous works, these authors conclude that magnetic interaction effectively locks the stellar rotation to about 10% the break-up velocity, a value which actually depends on the disk accretion rate and the stellar magnetic moment. While they correctly stress the importance of dealing with the exact balance between open and closed field lines and their corresponding angular momentum flux, the exact magnetospheric structure in the innermost region will certainly depend on the resistivity (diffusivity) of the disk and corona material. This is, however, not included in their treatment as an ideal MHD code has been applied.

We summarize this section noting that tremendous progress has occurred in the numerical simulation of the star-disk interaction. The role of numerical simulations is pivotal in this area because the mechanisms involved are complex, strongly interrelated, and often highly time-dependent. It is fair to say that numerical simulations of the star-disk interaction have not yet shown the launching of a jet flow comparable to the observations.

6. JETS AND GRAVITATIONAL COLLAPSE

Jets are expected to be associated with gravitational collapse because disks are the result of the collapse of rotating molecular cloud cores. One of the first simulations to show how jets arise during gravitational collapse is the work of *Tomisaka* (1998, 2002). Here, the collapse of a magnetized core within a rotating cylinder of gas gave rise the formation of a disk from which a centrifugally drive, disk wind was produced. Analytical work by *Krasnopolksy and Königl* (2002) provides an interesting class of self-similar solutions for the collapse of rotating, magnetized, isothermal cores including ambipolar diffusion that could be matched onto BP82 outflows.

Given the importance of Bonner-Ebert (B-E) spheres in the physics of star formation and gravitational collapse, recent efforts have focused on understanding the evolution of magnetized B-E spheres. Whereas purely hydrodynamic collapses of such objects never show outflows (e.g., *Foster and Chevalier*, 1993; *Banerjee et al.*, 2004), the addition of a magnetic field produces them. *Matsumoto and Tomisaka* (2004) have studied the collapse of rotating B-E spheres wherein the magnetic axis is inclined with the initial rotation axis. They observe that after the formation of an adiabatic core, outflow is ejected along the local magnetic field lines. Eventually, strong torques result in the rapid alignment of the rotation and magnetic field vectors.

The collapse of a magnetized, rotating, B-E sphere with molecular cooling included (but not dust), was carried out by *Banerjee and Pudritz* (2006) using the FLASH adaptive mesh refinement code. The results of this simulation are shown in Fig. 5 which shows the end state (at about 70,000 yrs) of the collapse of a B-E sphere that is chosen to be

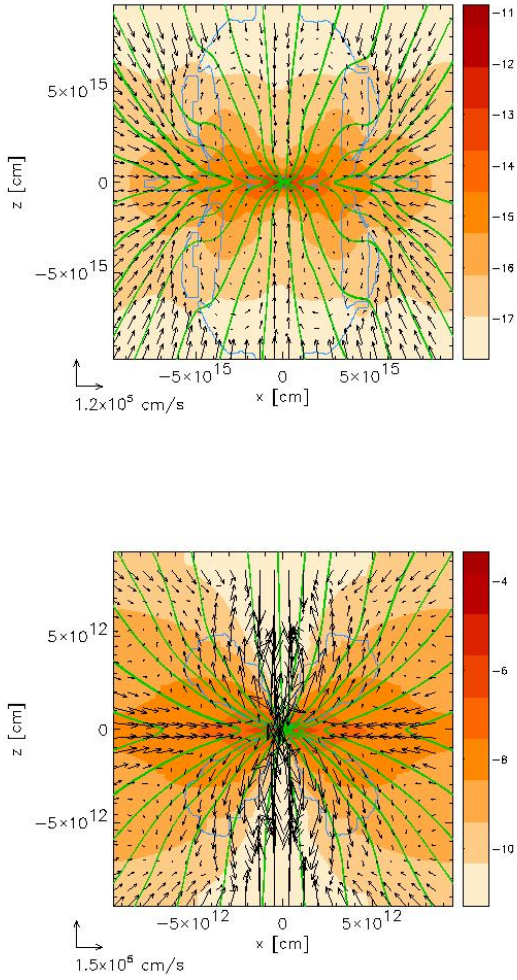


Fig. 5.— Large scale outflow (top frame, scale of hundreds of AU), and and small scale disk wind and jet formed (bottom frame, scale of a fraction of an AU) during the gravitational collapse of a magnetized B-E, rotating cloud core. Cross-sections through the disk and outflows are shown – the blue contour marks the Alfvén surface. Snapshots taken of an Adaptive Mesh calculation at about 70,000 years into the collapse. [Adapted from *Banerjee and Pudritz, 2006*].

precisely the Bok globule observed by *Alves et al. (2001)* – whose mass is $2.1 M_{\odot}$ and radius $R = 1.25 \times 10^4$ AU at an initial temperature of 16 K. Two types of outflow can be seen: (i) an outflow that originates at scale of $\simeq 130$ AU on the forming disk that consists of a wound up column of toroidal magnetic field whose pressure gradient pushes out a slow outflow; and (ii) a disk-wind that collimates into a jet on scale of 0.07 AU. A tight proto-binary system has formed in this simulation, whose masses are still very small $\leq 10^{-2} M_{\odot}$, which is much less than the mass of the disk at this time $\simeq 10^{-1} M_{\odot}$. The outer flow bears the hallmark

of a magnetic tower, first observed by *Uchida and Shibata*, and studied by *Lynden-Bell (2003)*. Both flow components are unbound, with the disk wind reaching 3 km s^{-1} at 0.4 AU which is quite super-Alfvénic and above the local escape speed. The outflow and jet speeds will increase as the central mass grows.

We conclude that the theory and computation of jets and outflows is in excellent agreement with new observations of many kinds. Disk winds are triggered during magnetized collapse and persist throughout the evolution of the disk. They efficiently tap accretion power, transport a significant part portion of the disk's angular momentum, and can achieve different degrees of collimation depending on their mass loading. Accretion-powered stellar winds may also solve the stellar angular momentum problem. We are optimistic that observations will soon be able to test the universality of outflows, all the way from circumplanetary disks to those around O stars.

Acknowledgments. We are indebted to Nordita for hosting an authors' meeting, Tom Ray for stimulating discussions, Robi Banerjee and Bo Reipurth for careful reads of the manuscript, and an anonymous referee for a very useful report. The research of REP and RO is supported by grants from NSERC of Canada. C.F. acknowledges travel support by the German science foundation to participate in the PPV conference.

REFERENCES

- Afshordi N., Mukhopadhyay B., and Narayan R. (2005) *Astrophys. J.*, 629, 373-382.
 Alves J. F., Lada C. J., and Lada E. A. (2001) *Nature*, 409, 159-161.
 Anderson J. M., Li Z.-Y., Krasnopol'sky R., and Blandford R. D. (2003) *Astrophys. J.*, 590, L107-L110.
 Anderson J. M., Li Z.-Y., Krasnopol'sky R., and Blandford R. D. (2005) *Astrophys. J.*, 630, 945-957.
 Bacciotti F., Mundt R., Ray T. P., Eislöffel J., Solf J., and Camenzind M. (2000) *Astrophys. J.*, 537, L49-L52.
 Bacciotti F., Ray T. P., Mundt R., Eislöffel J., and Solf J. (2002) *Astrophys. J.*, 576, 222-231.
 Bacciotti F., Ray T. P., Eislöffel J., Woitas J., Solf J., Mundt R., and Davis C. J. (2003) *Astrophys. Space Sci.* 287, 3-13.
 Bacciotti F. (2004) *Astrophys. Space Sci.* 293, 37-44.
 Balbus S. A., Hawley J. F., and Stone J. M. (1996) *Astrophys. J.*, 467, 76-86.
 Banerjee R. and Pudritz R. E. (2006) *Astrophys. J.*, 641, April 20.
 Banerjee R., Pudritz R. E., and Holmes L. (2004) *Mon. Not. R. Astron. Soc.*, 355, 248-272.
 Bardou A., Rekowsky B. v., Dobler W., Brandenburg A., and Shukurov A. (2001) *Astron. Astrophys.*, 370, 635-648.
 Bateman G. (1980) *Magneto-Hydrodynamical Instabilities*, MIT Press, Cambridge.
 Blandford R. D. and Payne D. G. (1982) *Mon. Not. R. Astron. Soc.*, 199, 883-903.
 Boldyrev S. and Cattaneo F. (2004) *Phys. Rev. Lett.*, 92, 144501.
 Bourke T. L., Crapsi A., Myers P. C., Evans N. J., et al. (2005) *Astrophys. J.*, 633, L129-L132.
 Brandenburg A. and Sokoloff D. (2002) *Geophys. Astrophys. Fluid Dynam.*, 96, 319-344.

- Brandenburg A. and Subramanian K. (2005) *Phys. Rep.*, **417**, 1-209.
- Brandenburg A., Nordlund Å., Stein R. F., and Torkelsson, U. (1995) *Astrophys. J.*, **446**, 741-754.
- Cabrit S., Raga A. C., and Gueth F. (1997) In *Herbig-Haro Flows and the Birth of Low Mass Stars* (B. Reipurth and C. Bertout, eds.), pp. 163-180. Dordrecht, Kluwer.
- Camenzind M. (1990) *Reviews in Modern Astronomy*, **3**, 234-265.
- Campbell C. G. (2000) *Mon. Not. R. Astron. Soc.*, **317**, 501-527.
- Campbell C. G. (2003) *Mon. Not. R. Astron. Soc.*, **345**, 123-143.
- Campbell C. G., Papaloizou J. C. B., and Agapitou V. (1998) *Mon. Not. R. Astron. Soc.*, **300**, 315-320.
- Cao X. and Spruit H. C. 1994, *Astron. Astrophys.*, **287**, 80-86.
- Casse F. and Ferreira J. (2000) *Astron. Astrophys.*, **353**, 1115-1128.
- Casse F. and Keppens R. (2002) *Astrophys. J.*, **581**, 988-1001.
- Casse F. and Keppens R. (2004) *Astrophys. J.*, **601**, 90-103.
- Chagelishvili G. D., Zahn J.-P., Tevzadze A. G., and Lominadze, J. G. (2003) *Astron. Astrophys.*, **402**, 401-407.
- Chiang E. I., Joung M. K., Creech-Eakman M. J., Qi C., Kessler J. E., Blake G. A., and van Dishoeck E. F. (2001) *Astrophys. J.*, **547**, 1077-1089.
- Cowling T. G. (1934) *Mon. Not. R. Astron. Soc.*, **94**, 39-48.
- De Villiers J.-P., Hawley J. F., Krolik J. H., and Hirose S. (2005), *Astrophys. J.*, **620**, 878-888.
- Donati J.-F., Paletou F., Bouvier J., and Ferreira J. (2005), *Nature*, **438**, 466-469.
- Dubrulle B., Marie L., Normand C., Richard D., Hersant F., and Zahn J.-P. (2005) *Astron. Astrophys.*, **429**, 1-13.
- Eichler D. (1993), *Astrophys. J.*, **419**, 111-116.
- Fendt C. (2005), *Astrophys. J.*, submitted (astro-ph/0511611).
- Fendt C. and Camenzind M. (1996), *Astron. Astrophys.*, **313**, 591-604.
- Fendt C. (2003) *Astron. Astrophys.*, **411**, 623-635.
- Fendt C. and Elstner D. (1999) *Astron. Astrophys.*, **349**, L61-L64.
- Fendt C. and Elstner D. (2000) *Astron. Astrophys.*, **363**, 208-222.
- Fendt C. and Čemeljić, M. (2002) *Astron. Astrophys.*, **395**, 1045-1060.
- Ferreira J. (1997) *Astron. Astrophys.*, **319**, 340-359.
- Ferreira J. and Casse F. (2004) *Astrophys. J.*, **601**, L139-L142.
- Fleming T. and Stone J. M. (2003) *Astrophys. J.*, **585**, 908-920.
- Foster, P. N. and Chevalier, R. A. (1993) *Astrophys. J.*, **416**, 303-311.
- Fromang S., Terquem C., and Balbus S. A. (2002) *Mon. Not. R. Astron. Soc.*, **329**, 18-28.
- Gammie C. F. (1996) *Astrophys. J.*, **457**, 355-362.
- Goodman J. and Rafikov R. R. (2001) *Astrophys. J.*, **552**, 793-802.
- Goodson A. P., Winglee R. M., and Böhm K.-H. (1997) *Astrophys. J.*, **489**, 199-209.
- Goodson A. P., Böhm K.-H., and Winglee R. M. (1999) *Astrophys. J.*, **524**, 142-158.
- Goodson A. P. and Winglee R. M. (1999) *Astrophys. J.*, **524**, 159-168.
- Greenhill L. J., Gwinn C. R., Schwartz C., Moran J. M., and Diamond, P. J. (1998) *Nature*, **396**, 650-653.
- Hardee P. and Rosen A. (1999) *Astrophys. J.*, **524**, 650-666.
- Hawley J. F., Balbus S. A., and Winters W. F. (1999) *Astrophys. J.*, **518**, 394-404.
- Hawley J. F. (2000) *Astrophys. J.*, **528**, 462-479.
- Hayashi M. R., Shibata K., and Matsumoto R. (1996) *Astrophys. J.*, **468**, L37-L40.
- Herbst W., Bailer-Jones C. A. L., Mundt R., Meisenheimer K., and Wackermann R. (2002) *Astron. Astrophys.*, **398**, 513-532.
- Heyvaerts J. (2003) In *Accretion discs, jets, and high energy phenomena in astrophysics*, (V. Beskin, et al., eds.), p. 3., Springer-Verlag, Berlin.
- Heyvaerts J. and Norman C. (1989) *Astrophys. J.*, **347**, 1055-1081.
- Inutsuka S.-I. and Sano T. (2005) *Astrophys. J.*, **628**, L155-L158.
- Keppens R. and Goedbloed J. P. (2000) *Astrophys. J.*, **530**, 1036-1048.
- Kigure H. and Shibata K. (2005) *Astrophys. J.*, **634**, 879-900.
- Kley W. and Lin D. N. C. (1992) *Astrophys. J.*, **397**, 600-612.
- Kley W., D'Angelo G., and Henning T. (2001) *Astrophys. J.*, **547**, 457-464.
- Königl A. (1991) *Astrophys. J.*, **370**, L39-L43.
- Königl A. (1999) *New Astron. Rev.*, **43**, 67-77.
- Königl A. (2004) *Astrophys. J.*, **617**, 1267-1271.
- Königl A. and Choudhuri A. R. (1985) *Astrophys. J.*, **289**, 173-187.
- Königl A. and Pudritz R. E. (2000) In *Protostars and Planets IV* (V. Mannings et al., eds.), p. 759 - 787. Univ. of Arizona, Tucson.
- Krasnopol'sky R. and Königl A. (2002) *Astrophys. J.*, **580**, 987-1012.
- Krasnopol'sky, R., Li Z.-Y., and Blandford R. D. (1999) *Astrophys. J.*, **526**, 631-642.
- Krasnopol'sky, R., Li Z.-Y., and Blandford R. D. (2003) *Astrophys. J.*, **595**, 631-642.
- Krumholz M. R., McKee C. F., and Klein R. I. (2005) *Astrophys. J.*, **618**, L33-L36.
- Kudoh T., Matsumoto R., and Shibata K. (1998) *Astrophys. J.*, **508**, 186-199.
- Küker M., Henning T., and Rüdiger G. (2003) *Astrophys. J.*, **589**, 397-409; erratum: *Astrophys. J.*, **614**, 526.
- Kuwabara T., Shibata K., Kudoh T., and Matsumoto, R. (2005) *Astrophys. J.*, **621**, 921-931.
- Lai D. (1999) *Astrophys. J.*, **524**, 1030-1047.
- Lai D. (2003) *Astrophys. J.*, **591**, L119-L122.
- Lee C.-F., Mundy L. G., Reipurth B., Ostriker E. C., and Stone, J. M. (2000) *Astrophys. J.*, **542**, 925-945.
- Lesur G. and Longaretti P.-Y. (2005) *Astron. Astrophys.*, **444**, 25-44.
- Li Z.-Y. (1995) *Astrophys. J.*, **444**, 848-860.
- Li Z.-Y. (1996) *Astrophys. J.*, **465**, 855-868.
- Long M., Romanova M. M., and Lovelace, R. V. E. (2005) *Astrophys. J.*, **634**, 1214-1222.
- Lubow S. H., Papaloizou J. C. B., and Pringle J. E. (1994) *Mon. Not. R. Astron. Soc.*, **268**, 1010-1014.
- Lucek S. G. and Bell A. R. (1996) *Mon. Not. R. Astron. Soc.*, **281**, 245-256.
- Lynden-Bell D. (2003) *Mon. Not. R. Astron. Soc.*, **341**, 1360-1372.
- Matsumoto R., Uchida Y., Hirose S., Shibata K., Hayashi M. R., Ferrari A., Bodo G., and Norman C. (1996) *Astrophys. J.*, **461**, 115-126.
- Matsumoto T. and Tomisaka K. (2004) *Astrophys. J.*, **616**, 266-282.
- Matsumura S. and Pudritz R. E. (2005) *Astrophys. J.*, **618**, L137-L140.
- Matsumura S. and Pudritz R. E. (2006) *Mon. Not. R. Astron. Soc.*, **365**, 572-584.
- Matt S. and Pudritz R. E. (2005a) *Mon. Not. R. Astron. Soc.*, **356**, 167-182.
- Matt S. and Pudritz, R. E. (2005b) *Astrophys. J.*, **632**, L135-L138.

- Matt S., Goodson A. P., Winglee R. M., and Bořík K.-H. (2002) *Astrophys. J.*, 574, 232-245.
- Ménard F. and Duchêne G. (2004) *Astron. Astrophys.*, 425, 973-980.
- Meier D. L., Edgington S., Godon P., Payne D. G., and Lind, K. R. (1997) *Nature*, 388, 350-352.
- Michel F. C. (1969) *Astrophys. J.*, 158, 727-738.
- Miller K. A. and Stone J. M. (1997) *Astrophys. J.*, 489, 890-902.
- Miller K. A. and Stone J. M. (2000) *Astrophys. J.*, 376, 214-419.
- Molemaker M. J., McWilliams J. C., and Yavneh I. (2001) *Phys. Rev. Lett.*, 86, 5270-5273.
- Nakamura M., Uchida Y., and Hirose S. (2001) *New Astron.*, 6, 61-78.
- Nakamura M. and Meier D. (2004) *Astrophys. J.*, 617, 123-154.
- Ouyed R. and Pudritz R. E. (1997a) *Astrophys. J.*, 482, 712-732 (OPI).
- Ouyed R. and Pudritz R. E. (1997b) *Astrophys. J.*, 484, 794-809 (OPII).
- Ouyed R., Pudritz R. E., and Stone, J. M. (1997) *Nature*, 385, 409-414 (OPS).
- Ouyed R. and Pudritz R. E. (1999) *Mon. Not. R. Astron. Soc.*, 309, 233-244 (OPIII).
- Ouyed R., Clarke D. A., and Pudritz R. E. (2003) *Astrophys. J.*, 582, 292-319 (OCP).
- Ouyed R. (2003) *Astrophys. Space Sci.*, 287, 87-97.
- O'Sullivan M., Truss M., Walker C., Wood K., Matthews O., et al. (2005) *Mon. Not. R. Astron. Soc.*, 358, 632-640.
- Pelletier G. and Pudritz R. E. (1992) *Astrophys. J.*, 394, 117-138.
- Pfeiffer H. P. and Lai D. (2004) *Astrophys. J.*, 604, 766-774.
- Pinte C. and Ménard F. (2004) In *The Search for Other Worlds* (S. S. Holt and D. Demings, eds.), pp. 123-126. American Institute of Physics.
- Pringle J. E. (1996) *Mon. Not. R. Astron. Soc.* 281, 357-361.
- Pudritz R. E. (2003) In *Accretion discs, jets, and high energy phenomena in astrophysics*, (V. Beskin, et al., eds.), p. 187 - 230. Springer-Verlag, Berlin.
- Pudritz R. E. and Banerjee B. (2005) In *Massive star birth: A crossroads of Astrophysics*, R. Cesaroni, M. Felli, E. Churchwell, and M. Walmsley eds., pp.163-173, Cambridge University, Cambridge.
- Pudritz R. E., Rogers C., and Ouyed R. (2006) *Mon. Not. R. Astron. Soc.*, 365, 1131-1148.
- Pudritz R. E. and Norman C. A. (1983) *Astrophys. J.*, 274, 677-697.
- Pudritz R. E. and Norman C. A. (1986) *Astrophys. J.*, 301, 571-586.
- Quillen A.C. and Trilling D. E. (1998) *Astrophys. J.*, 508, 707-713.
- von Rekowski B., Brandenburg A., Dobler W., and Shukurov A. (2003) *Astron. Astrophys.*, 398, 825-844.
- von Rekowski B. and Brandenburg A. (2004) *Astron. Astrophys.*, 420, 17-32.
- von Rekowski B. and Brandenburg A. (2006) *Astron. Nachr.*, 327, 53-71.
- Roberts P. H. (1967) *Introduction to Magneto-Hydrodynamics*, Longmans, London.
- Romanova M. M., Ustyugova G. V., Koldoba A. V., Chechetkin V. M., and Lovelace R. V. (1997) *Astrophys. J.*, 482, 708-711.
- Romanova M. M., Ustyugova G. V., Koldoba A. V., Chechetkin V. M., and Lovelace R. V. E. (1998) *Astrophys. J.*, 500, 703-713.
- Romanova M. M., Ustyugova G. V., Koldoba A. V., and Lovelace R. V. E. (2002) *Astrophys. J.*, 578, 420-438.
- Romanova M. M., Toropina O. D., Toropin Y. M., and Lovelace R. V. E. (2003) *Astrophys. J.*, 588, 400-407.
- Romanova M. M., Ustyugova G. V., Koldoba A. V., and Lovelace R. V. E. (2004) *Astrophys. J.*, 610, 920-932.
- Różyczka M. and Spruit H. C. 1993, *Astrophys. J.*, 417, 677-686.
- Sano T., Miyama S. M., Umebayashi T., and Nakano T. (2000) *Astrophys. J.*, 543, 486-501.
- Sano T. and Stone, J. M. (2002) *Astrophys. J.*, 570, 314-328.
- Schandl S. and Meyer F. (1994) *Astron. Astrophys.*, 289, 149-161.
- Schekochihin A. A., Haugen N. E. L., Brandenburg A., Cowley S. C., Maron J. L., and McWilliams J. C. (2005) *Astrophys. J.*, 625, L115-L118.
- Semenov D., Wiebe D., and Henning, T. (2004) *Astron. Astrophys.*, 417, 93-106.
- Shakura N. I. and Sunyaev R. A. (1973) *Astron. Astrophys.*, 24, 337-355
- Shalybkov D. and Rüdiger G. (2005) *Astron. Astrophys.*, 438, 411-417.
- Shibata K. and Uchida Y. (1986) *Publ. Astron. Soc. Japan*, 38, 631-660.
- Shu F. H., Najita J. R., Shang H., and Li Z.-Y. (2000) In *Protostars and Planets IV* (V. Mannings et al., eds.), p. 789 - 813. Univ. of Arizona, Tucson.
- Shu F., Najita J., Ostriker E., Wilkin F., Ruden S., and Lizano S. (1994) *Astrophys. J.*, 429, 781-796.
- Spruit H. C., Foglizzo T., and Stehle R. (1997) *Mon. Not. R. Astron. Soc.*, 288, 333-342.
- Spruit H. C. and Uzdensky D. A. (2005) *Astrophys. J.*, 629, 960-968.
- Stone J. M., Hawley J. F., Gammie C. F., and Balbus S. A. (1996) *Astrophys. J.*, 463, 656-673.
- Stone J. M. and Norman M. L. (1992) *Astrophys. J. Suppl.*, 80, 753-790.
- Stone J. M. and Norman M. L. (1994) *Astrophys. J.*, 433, 746-756.
- Symington N. H., Harries T. J., and Kurosawa R. (2005a) *Mon. Not. R. Astron. Soc.*, 356, 1489-1500.
- Symington N. H., Harries T. J., Kurosawa R., and Naylor T. (2005b) *Mon. Not. R. Astron. Soc.*, 358, 977-984.
- Todo Y., Uchida Y., Sato T., and Rosner R. (1993) *Astrophys. J.*, 403, 164-174.
- Tomisaka K. (1998) *Astrophys. J.*, 502, L163-L167.
- Tomisaka K. (2002) *Astrophys. J.*, 575, 306-326.
- Turner N. J. (2004) *Astrophys. J.*, 605, L45-L48.
- Uchida Y. and Shibata K. (1984) *Publ. Astron. Soc. Japan*, 36, 105-118.
- Uchida Y. and Shibata K. (1985) *Proc. Astron. Soc. Japan*, 37, 515-535.
- Uchida Y., McAllister A., Strong K. T., Ogawara Y., Shimizu T., Matsumoto R., and Hudson H. S. (1992) *Proc. Astron. Soc. Japan*, 44, L155-L160.
- Umurhan O. M. (2006) *Mon. Not. R. Astron. Soc.*, 365, 85-100.
- Uzdensky D. A., Königl A., and Litwin C. (2002) *Astrophys. J.*, 565, 1191-1204.
- Vitorino B. F., Jatenco-Pereira V., and Opher R. (2002) *Astron. Astrophys.*, 384, 329.
- Wardle M. and Königl A. (1993) *Astrophys. J.*, 410, 218-238.
- Woitas J., Ray T. P., Bacciotti F., Davis C. J., and Eislöffel J. (2002) *Astrophys. J.*, 580, 336-342.
- Wu Y., Wei Y., Zhao M., Shi Y., Yu W., Qin S., and Huang M. (2004) *Astron. Astrophys.*, 426, 503-515.
- Ziegler U. and Rüdiger G. (2000) *Astron. Astrophys.*, 356, 1141-1148.